Synthesis of chemical tools to study the immune system

Graaff, M.J. van de

Note: To cite this publication please use the final published version (if applicable).

Chapter 5

General summary and future prospects[1,2]

General Summary

Toll-like receptors (TLRs) are important sensors partaking in the initiation and propagation of an immune response. This makes synthetic TLR ligands potential therapeutic targets for diseases in which a correctly mounted immune response is beneficial for host survival, such as in preventing or treating infections.[3,4] TLRs are also increasingly investigated in the context of immune-based treatment of cancers.[5] TLR-ligand-based therapies are, however, not without risk: an improperly triggered immune response through TLR activation can lead to excessive inflammation, which in turn can result in sepsis[6], asthma[7] and auto-immune disease.[8] A clear understanding of the signaling pathways that emerge following TLR liganding is therefore vital in rationally designing therapeutics that exploit the TLR system. In this manner, beneficial effects can be invoked, whilst immune-related pathology can be avoided.

Over the past decade, TLRs have been shown to display complex, dynamic behaviour. For example, organelle-specific activation has been described to prevent the detection of self-ligands.[9–12] Moreover, certain TLRs have been shown to tailor their signaling outcome, depending on the subcellular site of activation. For example, activation of TLR4 when localized on the plasma membrane ultimately results in a pro-inflammatory response, whereas antiviral type I interferons are produced upon activation of TLR4 residing in endosomes.

Various chemical tools have been developed to study spatiotemporal effects on TLR-signaling. For example, TLR ligands immobilized on surfaces through biotin-streptavidin interactions can be used the activation of TLRs exclusively at the plasma membrane.[13] Activating the TLRs at a specific intracellular location has not yet been achieved. In a first step towards achieving this, photolabile protecting groups ('photocages') have been introduced on crucial functionalities within TLR ligands and light has been used to activate the ligands.[14–17] Whereas this has provided some control over receptor signaling in time, phototoxicity of the UV-light needed to activate these 'pro-ligands' as well as low spatial restriction are current limitations that need to be overcome to obtain spatiotemporal insights.

This thesis has explored the use of less-toxic approaches to induce deprotection of TLR pro-ligands *in vitro*. The aim was to develop methods that would allow the study of TLR-ligands described above, whilst circumventing the limitations set by a photo-irradiation mediated strategy. The first approach that was explored entailed the use of recently-published photocages with superior photochemical properties compared to those previously reported. It was explored whether the use of protecting groups that could be removed by low-dose visible light, and/or two-photon excitation, could upon the previously reported photoprotecting groups. A second approach that was explored in this thesis employed chemically-removable protecting groups. Here, small molecules were used

to remove the protecting groups instead of light, offering an alternative strategy towards sub-cellular activation of TLR-ligands.

Chapter 1 gives a literature overview on the role of pattern-recognition receptors (PRRs) in immune activation. The role of TLRs as a subset of the PRRs is discussed and a short literature review is provided on the signaling biology of these receptors. The chemical structures of the receptor agonists are also described, as well as the concept of caging the activity of these agonists to yield better understanding of the signaling biology. The chapter ends with a brief overview on the currently available photocages and potential chemical caging approaches.

Chapter 2 describes the synthesis of a *trans*-cyclooctene (TCO) protected Pam_2CSK_4, in which the TCO-group could serve as a chemically removable protecting group. This compound was shown to bind to TLR2 similar to the unprotected Pam2CSK4 ligand, whilst preventing subsequent dimerization of the bound TLR2 with TLR6 (thereby preventing activation). TLR-signaling could be activated by first priming a mouse macrophage cell line with TCO-Pam_2CSK_4 followed by the subsequent addition of a tetrazine derivative that removes the TCO-group by means of an inverse electron-demand Diels-Alder reaction, followed by retro-Diels-Alder, rearrangement and elimination steps. The activation of immune cells under this condition was visualized by imaging the nuclear translocation of GFP-labelled NF-κB and further confirmed using a reporter cell line which expressed an alkaline phosphatase reporter under the NF-κB- promotor.

Interestingly, human cell lines exhibited significant TLR2/6 activation even in the absence of the deprotecting tetrazine. To reduce this background activation, various modifications to the ligand and TCO were explored. It was found that hydrophilic and bulky variants of the TCO protecting group did not reduce this residual activity. Substitution of the tetralysine peptide for a triethylene glycol did reduce background activation of the protected TLR2/6 ligand. This new ligand allowed the precise temporal control over TLR2/6 activation, as near-identical nuclear translocation rates of nuclear NF-κB were observed by human macrophages cell lines treated with free ligand compared to those pre-treated with caged ligands and activated by the addition of tetrazine.

Chapter 3 describes efforts towards applying the TCO-tetrazine elimination approach to TLR4, 7/8 and 9 ligands. TCO-groups were installed on critical functionalities within each of these TLR's ligand. For TLR9, a CpG-ODN was synthesized in which the cytidine nucleobase was caged with a TCO on its exocyclic amine. To this end, a DMTr/phosphoramidite-protected cytosine building block was synthesized with the TCO installed on its nucleobase. This was used in the on-resin synthesis of ODN. Using this building block, a 12- and 20-meric CpG ODN was synthesized with either an unprotected cytosine or TCO-protected cytosine in the CpG sequence. Its ability to effectively induce TLR9 activation upon co-administering tetrazine is currently awaiting assessment.

The TLR7/8-ligand Resiquimod was also caged with a TCO on its exocyclic amine. This yielded a caged ligand of which the activity could be controlled by tetrazine addition. This was assessed by measuring IL6 and TNFα secretion by bone marrow-derived macrophages (BMDMs). Furthermore, the bis-functionalized TCO-$(OSu)_2$ reagent was used to synthesize Resiquimod-TCO-OSu, of which its immolative end was appended to the TLR7/8 ligand and the non-

immolative end was appended to the anti-tumour antibody TA99. This reagent was used to deliver TLR ligands to a melanoma *in vivo*, with induced TLR-activity as the result.

Finally, a synthetic pyrimido[5,4-*b*]indole TLR4 ligand was caged with TCO on the endocyclic indole amine, which prevented the activation of TLR4 in BMDMs. The TNFα secretion by BMDMs was blocked by this TCO-modification and could be reactivated upon the addition of tetrazine. IL6 secretion, however, appeared not blocked by TCO-modification.

Chapter 4 describes the application of photocages in the development of light-controllable TLR-ligands. First, the TLR7 ligand 9-benzyl-8-oxo-2-butoxyadenine was protected with the NVOC-photocage on its exocyclic amine. The development of triethylene glycol monomethylether-modified NVOC was necessary to solubilize the construct, as modification with NVOC yielded an insoluble product. The effectivity of the ethylene glycol-modified NVOC to shield the ligand's activity towards TLR7 is currently awaiting assessment.

Next, the TLR2/6 ligand Pam_2CSK_4 was caged on its N-terminal amine with the two-photon-sensitive photocage 4-nitrophenyl(benzofuran) (NPBF). The ability to control ligand activity with this group was verified in THP1 Dual cells. Similar to the experiments outlined in Chapter 2, background activation was a problem with this ligand. The same solution as in Chapter 2 was applied, resulting in the NPBF-caged ligand Pam_2CS(*TEG*), in which the C-terminal tetralysine motif was replaced with a triethylene glycol motif. However, this ligand appeared insoluble in aqueous media and showed high adherence to plastic surfaces. This issue was addressed by the design and synthesis of a phenol-containing NPBF-analogue. The phenol functionality was exploited to include a variety of linkers that can be used to influence the physical-chemical properties of the cage, such as its water solubility. A carboxyl- and propargyl-carrying linker was used to decorate the phenol. Presence of the functionalized phenol also enhanced the molar attenuation efficiency ε by 30%.

Future prospects

The new dual cages, particularly the dual-functional NPBF-linker open up a wide range of future experiments, both within and beyond the TLR-field. For example, the NPBF-linked to a TLR-ligand may be used to generate a water-soluble variant of photocaged Pam_2CS(*TEG*), for application in experiments which exploit two-photon absorption to yield a high spatial accuracy. As proposed previously in literature[14], TLR2/6-bearing cells can be primed with a photocaged ligand and subsequently added to a different culture to study the propagation of an immune response (Figure **1**) after irradiation of a large group of murine cells. With this next iteration of photocaged TLR2/6 ligands, single-cell, and even single-endosome, activation could be within reach.
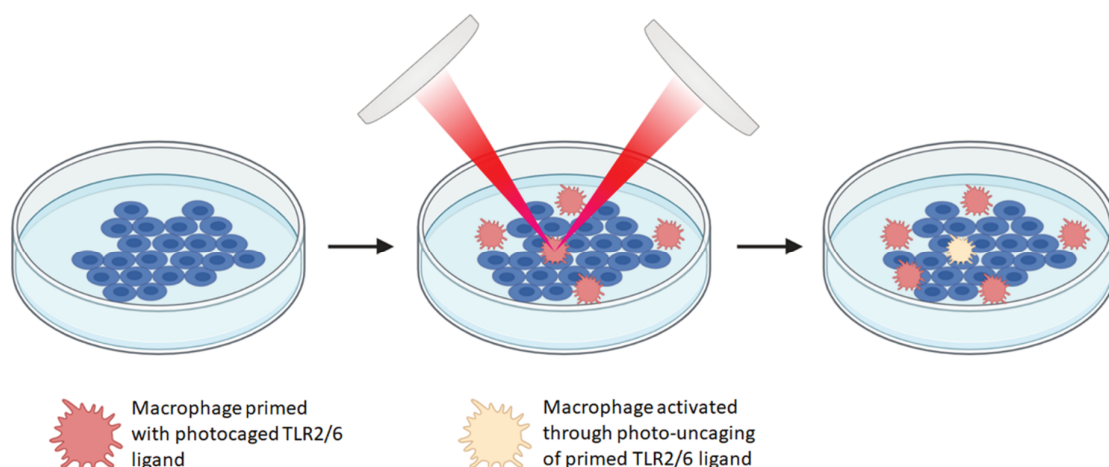
Figure 1. Macrophages primed with human-applicable NPBF-caged ligand can be added to a culture of cells to study the propagation of an immune response. Two-photon excitation enables single-cell activation, whereas the optimization of the TLR2/6 ligand in Chapter 2 enables its use in primary human cells.

The TCO-modified reagents can in future also be used to study spatially restricted activation. For example, by first pre-incubating a macrophage cell line with nanoparticles decorated with tetrazine to saturate their endo-lysosomal system, followed by the addition of the protected ligand, which will then only be deprotected inside the endolysosomal system (Figure **2**). Studying the phosphorylation of the signaling adapters under this condition will allow the isolation of only the intracellular signaling of the TLR2/6 receptor complex.
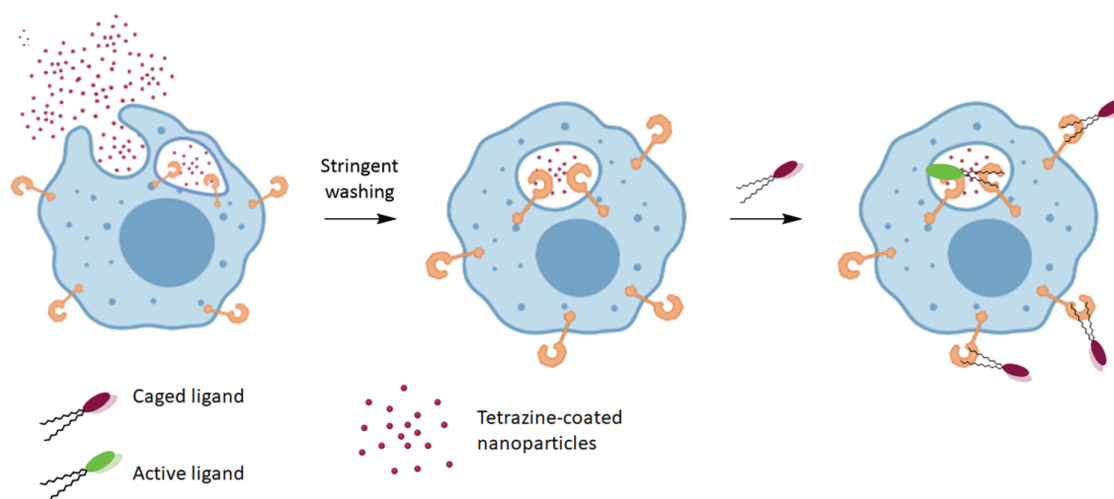

Figure 2. A strategy to activate intracellular TLRs. First the cells are treated with tetrazine-coated nanoparticles which are taken up through phago- and endocytic pathways. After a stringent washing procedure, the cells are treated with TCO-caged TLR-ligand. Liberation of the ligand from its cage should now be prevalent in intracellular vesicles as opposed to the extracellular environment.

Isolating the surface signal is also possible by for example immobilizing a tetrazine-biotin conjugate on a streptavidin-modified surface. Cells that are primed with TCO-caged ligand can then be exposed to this surface, after which the tetrazine will liberate the TCO from the ligand-receptor complex. The advantage of this approach – over the direct immobilization of the TLR-ligand – would be that the internalization of the receptor would not be negatively affected by the approach. After deprotection, the ligated TLR could be taken up as normal (Figure **3**).

Finally, in very recent work by the Fox-group[18], subcellular activation of the IEDDA reaction was achieved through the sub-cellular conversion of an unreactive dihydrotetrazine to a tetrazine using a photocatalyst and two-photon-excitation. Applying this approach to the generation of uncaging tetrazines *in vivo* would be an additional powerful tool to study localized TLR signaling.
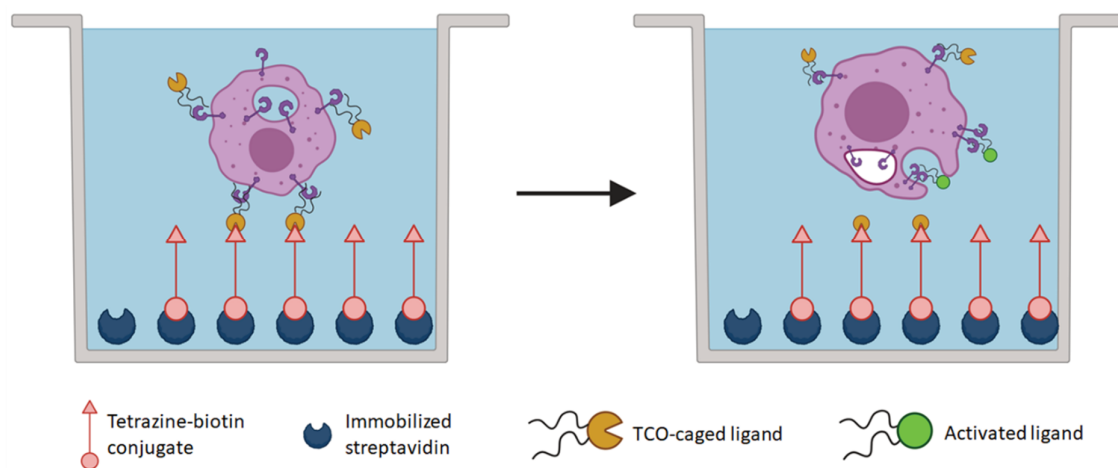

Figure 3. A more natural mode of surface-only TLR2/6 activation. A streptavidin-coated well is treated with a tetrazine-biotin conjugate. Then, cells primed with TCO-caged TLR2/6 ligand are added to the well. The tetrazine reacts with the TCO and liberates the ligand. TLR2/6 dimerization is initiated and endocytosis of the receptor proceeds naturally.

The photo- and chemo-cleavable linkers could in principle also be used to achieve the inverse of photoactivaton: photo-*de*activation. This would then allow the study of what happens if TLR-signaling is halted, rather than initiated. For this purpose, a photo-destructible TLR9 ligand may be designed. The palindromic TLR9-ligands reported by the group of Agrawal would for instance be a suitable starting point for this approach.[19] Agrawal and co-workers found that 5'-TCTGACGTTCT-X-TCTTGCAGTCT-5' (where X is a glyceryl linker) is a potent TLR9 agonist, whereas the bisectional sequence 5'-TCTGACGTTCT-3' is not. Substitution of the glyceryl linker by a photocleavable linker, such as the bis-functional TCO or NPBF could give rise to a TLR9 ligand that can effectively be switched off (Figure **4**). One possible caveat here is that the TCO-based linker may prove too labile to endure the synthetic cycles required to make the ligand. An NPBF-based linker on the other hand may be too difficult to deprotect quantitatively – a feature which is likely needed to completely terminate a TLR-mediated signaling event.
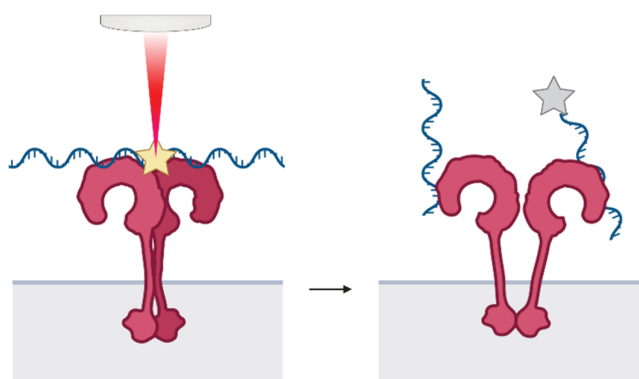
Figure 4. Concept of photodestructible TLR9 ligands. A CpG-containing oligodeoxynucleotide (ODN) is synthesized which possesses a photolabile linker in the appropriate position (fission must lead to non-binding fragments and the linker must not interfere with TLR9 binding). After binding of the conjugate with TLR9, the dimerized complex may be destabilized by cleavage of the photolinker, thus damping the signaling events stemming from the receptor-ligand complex.
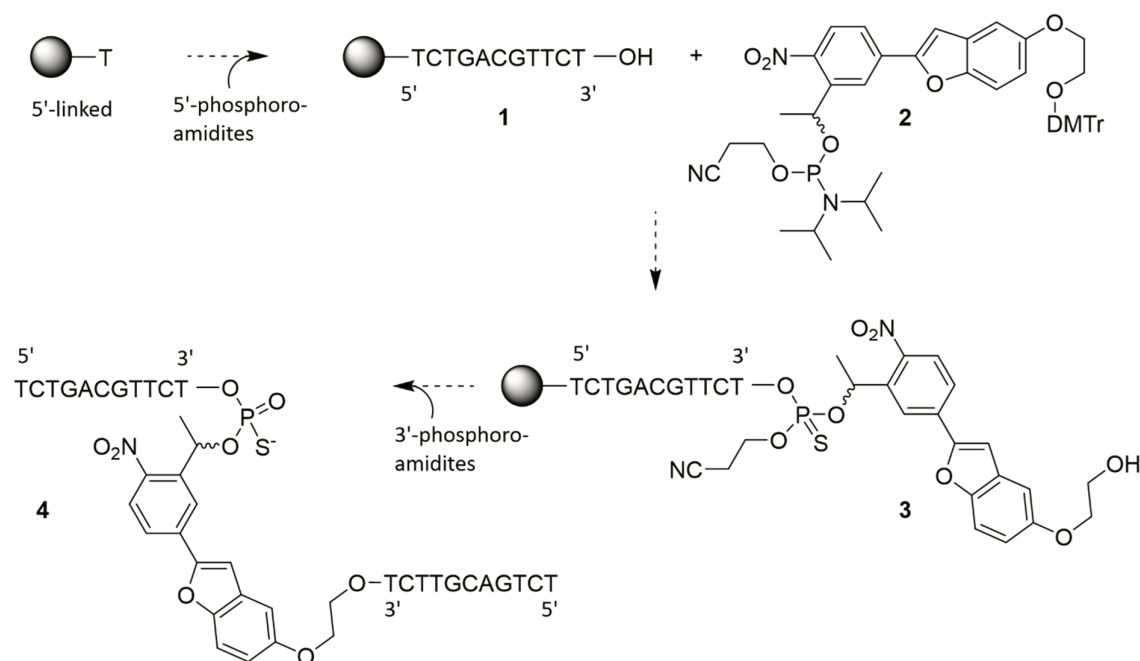
Scheme 1. Strategy for the synthesis of a photodestructible TLR9 ligand using the NPBF-linker. Oligonucleotide synthesis is first proceeded in the 5'→3' direction and the NPBF linker is installed in the bisectional position. Then, a 3'→5' direction is adopted to ultimately yield the photocleavable palindromic CpG ODN.

Application of photoresponsive linkers beyond TLR-ligands.

This thesis describes the use of the photocage NPBF in the study of TLR-activation.[20] However, these bifunctional photocages can also be employed for other purposes. During the work described in this thesis, the first steps in this direction were also taken: namely, through the design of a conjugate composed of a covalent proteasome inhibitor linked to a chemotherapeutic agent. This allowed the specific targeting of the caged toxin to multiple myeloma cells *in vitro,* followed by its

activation with low-dose photo-irradiation. The NPBF-linker was also used as a diagnostic tool in the development of a probe that could be used to mark CD8+ T cells in regions of interest (ROI) in a primary human tumour. This marking then enabled the isolation of the T-cells from the ROI, followed by their single-cell characterization.

Immunoproteasome inhibitor-doxorubicin conjugate[1]

Delivering a cytotoxic agent site-selectively to malignant neoplasms is an important strategy to reduce side-effects and to increase efficacy of chemotherapeutics. This is usually done by linking a drug of choice to an antibody. This can even be done in such a way that the drug is deactivated by the attachment of the linker. Localized immolation of the linker then reactivates the drug. This release of the drug can be achieved through either enzymatic activities[21], pH changes[22] or redox potential differences.[23,24] Alternatively, the release can be induced by an externally applied trigger, such as the addition of a tetrazine to a TCO-linked drug conjugate[25–27], or by applying a photon dose to a light-sensitive linker.[28] There are two major downsides to the use of antibodies for targeting. Firstly, the choice of target is limited to extracellular proteins only. This excludes many malignancies that do not possess such a unique defining feature. Secondly, surface antigens are usually only present at approximately 100,000 copies per cell. This makes the delivery of a therapeutic dose to the cell difficult.

Many malignancies are characterized by the upregulation of specific enzyme activities. It was envisaged that targeting such an enzyme with irreversible inhibitors could be a valuable alternative strategy, as the number of copies of an enzyme per cell is higher than for surface antigens, and the palette of targets that allow selective tumour targeting can be increased in this manner.

Here such an approach based on the photodestructible NPBF-linker is presented to target multiple myeloma cells *in vitro*. These cells have been shown to upregulate immunoproteasomes, whilst concomitantly downregulating constitutive proteasomes. The immunoproteasome inhibitor LU-035i targets the β5i subunit to induce proteolytic stress and eventually apoptosis in the target cell.[29] It is, however, known that these malignancies are able to evolve resistance to such a treatment. It was thus hypothesized that combining the immunoproteasome activity through an irreversible inhibitor with the release of a cytotoxic payload in the cells would reduce the change of resistance emerging. An immunoproteasome inhibitor-doxorubicin conjugate **6** was therefore designed (Figure **5**). The LU-035i group was envisaged to serve as both an immunoproteasome inhibitor and targeting group for delivering doxorubicin. This would provide a one-two-punch strategy to the multiple myeloma cells.
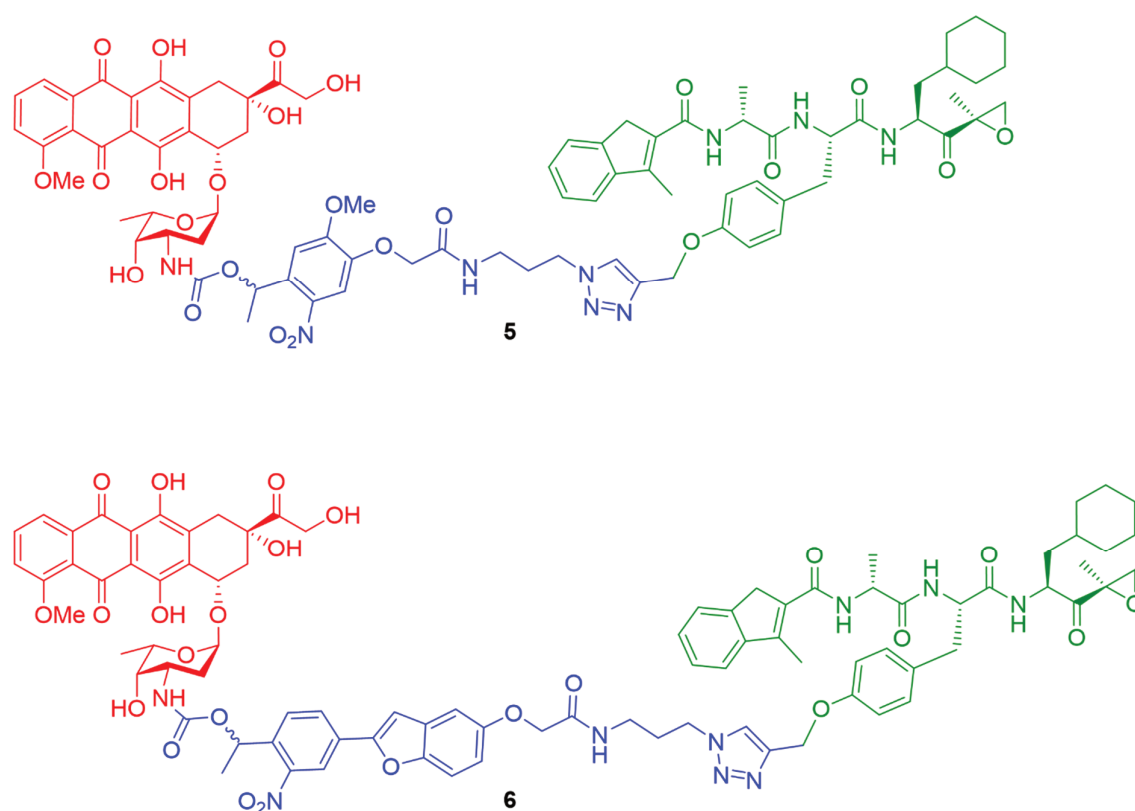
Figure 5. Conjugate consisting of doxorubicin (red) as a cytotoxic payload, bis-functionalized NVOC (blue, 5) or NPBF (blue, 6) as a self-immolative linker and LU-035i (green) as an immunoproteasome-targeting and -inhibiting warhead.

Conjugates **5** and **6** (Figure **5**) were made by conjugating the doxorubicin (doxo) amine through a carbamate to either photocleavable linker. It was previously reported that N-acyl derivatives of doxo are non-toxic.[22] LU-035i was conjugated to the photocleavable linkers through the tyrosine phenol, which has been shown not to affect its functionality.

A competitive activity-based protein profiling assay confirmed that both conjugates retained their subunit-selectivity (Figure **6**A). During initial kinetic experiments it was found that the uncaging rate of conjugate **5** was too low to be viable and was discarded from further assays. The uncaging rate of conjugate **6** at 10 µM was assessed at 375 nm and 420 nm (Figure **6**B) using LC-MS. Quantitative release was observed after 60 s of irradiation with 375 nm light. Phototoxicity of the two wavelengths towards AMO-1 cells was tested in a cell survivability assay (Figure **6**C) in which it was clear that the 420 nm light source was more harmful to cell survival. Therefore, further experiments were conducted using the 375 nm light source.
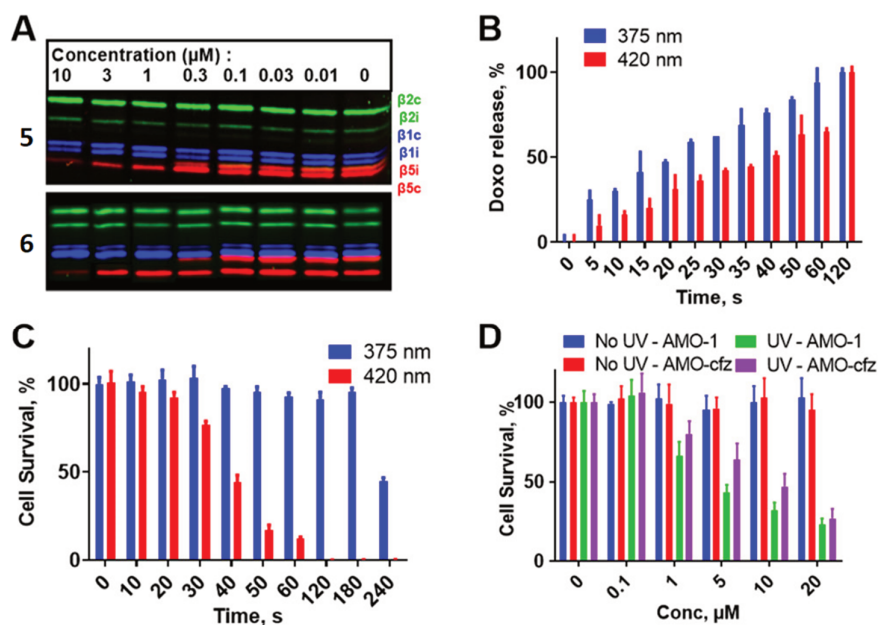
Figure 6. Biological evaluation of conjugates **5** and **6**. A) Validation of subunit-selectivity of the conjugates as well as their activity through a competitive activity-based protein profiling assay. B) Release of doxorubicin from conjugate **6** at 10 µM using two different wavelengths as quantified by LC-MS. C) Phototoxicity exhibited by both 375 nm and 420 nm irradiation on AMO-1 cells. D) Dose escalation of conjugate **6** in carfilzomib-sensitive (AMO-1) and carfilzomib-resistant (AMO-cfz) AMO-1 cells in the presence (UV) or absence (No UV) of 375 nm irradiation for 60 seconds. Experiment performed by Elmer Maurits.

The ability of conjugate **6** to induce apoptosis in AMO-1 cells was evaluated next. AMO-1 cells with an acquired resistance for Carfilzomib (an irreversible proteasome inhibitor currently used in the clinic to treat multiple myeloma patients) were also exposed to the conjugate. After treatment of the cells with the conjugate, cells were washed and irradiated for 60 s using 375 nm light. Cell survival was determined three days later (Figure **6**D). At a conjugate concentration of 10 µM more than 50% of both cell types were killed when exposed to irradiation.

The combined effect of proteolytic stress induced by LU-035i and poisoning of topoisomerase II by doxorubicin may overcome the resistance that can be acquired by malignant cells that are treated with proteasome inhibitors. This approach can be extended to other mechanism-based hydrolase inhibitors and combinations with highly cytotoxic agents. Although photodynamic therapy is already being applied in oesophageal and lung cancer, this work may aid in broadening the clinical opportunities within this field.[30]

Photoresponsive OR-gate[2]

Characterizing individual cells allows the study of functional diversity of a given cell population. Although techniques such as single-cell transcriptomics and proteomics are powerful tools to gain an in-depth understanding of cell states, spatial information is lost upon sample preparation. How environmental signals can influence cell state and differentiation can only be revealed when the spatial context is preserved. In tumours, for example, immune cells can be found in various regions

in the tumour, but how the cell states of these cells correlate to their localization remains poorly understood.[31]

Classical methods that are able to simultaneously determine the localization and phenotypes of individual cells, such as confocal microscopy and immunohistochemistry, are limited by the number of variables analysed. Other, state-of-the-art imaging techniques including multi-ion beam imaging by time of flight (MIBI-TOF)[32] and co-detection by indexing (CODEX)[33] do allow analysis of multiple markers on tissue slides. However, these methods are held back by the necessity to decide on which genes or proteins are assessed in advance and their spatial resolution. Analysis of single-cell transcriptomes with a high spatial accuracy has been achieved previously, using tissues from transgenic mouse models that express a photoactivatable green fluorescent protein and consequently switching these only in the regions of interest.[34] However, methods that necessitate the use of genetic encoding cannot be translated to analysis of primary human tissues. In response to this several approaches[35–40], including Slide-Seq[41], have emerged that enable the correlation of transcriptome data with cellular localization in human tissues. In these types of approaches the transcriptional activity can be analyzed in an unbiased manner, although the data output of gene-expression patterns is often obtained as averages of multiple cells. The specific labeling of cells in a confined region of interest, and consequent single-cell analysis of these cells is not hampered by this limitation, as exemplified by the recently developed ZipSeq method.[42]

In this work, it was postulated that an NPBF-based reagent could be used to locally 'mark' T-cells in a human primary tumour sample to allow for their subsequent single-cell profiling.
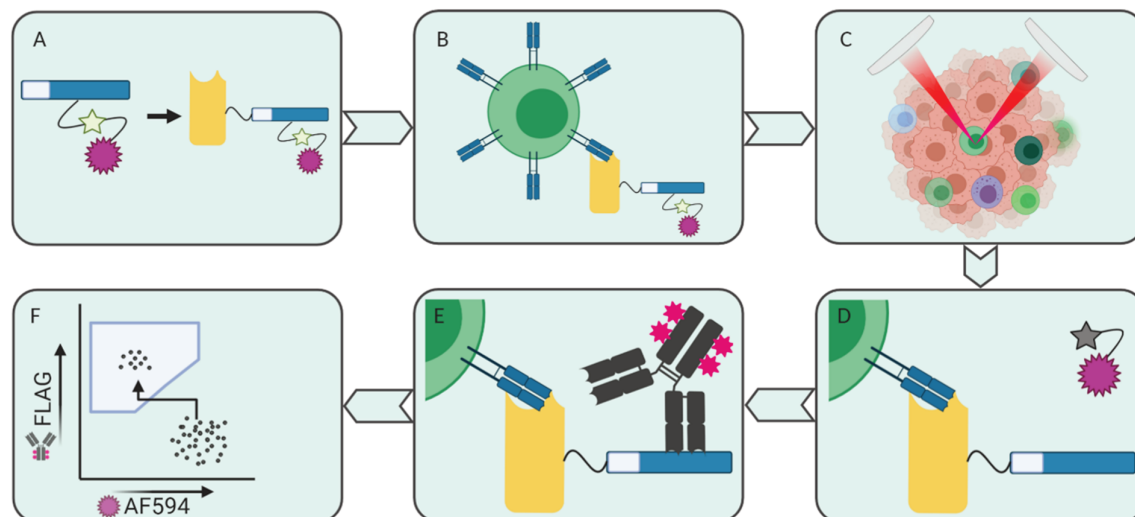

Figure 7. Strategy to tag and identify CD8+ T cells in a tumour sample. A) A peptide fragment containing a sortase recognition sequence (light blue) and a FLAG epitope (dark blue) is caged with a photocleavable linker (green star) containing an AF594 fluorophore (purple badge). This conjugate is ligated to an anti-CD8 nanobody through a sortase-mediated transpeptidation. B) The nanobody conjugate is applied to a tumour block containing CD8+ T cells and binds to CD8-sites. C) The tumour block is spatially-selective photo-irradiated with 405 nm light. D) Irradiation leads to release of the photolinker-fluorophore moiety, thus uncaging the FLAG-epitope. E) The tumour block is treated with fluorescently labeled anti-FLAG antibodies. F) The sample is sorted using FACS. Cells originating from regions-of-interest have been

irradiated and thus their AF594 'turned off' and simultaneously their FLAG signal 'turned on', leading to a two-dimensional separation.

The key feature of such a tagging reagent was designed to be a FLAG-tag (DYKDDDDK). This peptide epitope can readily be visualized by staining with a variety of specific antibodies. It also contains multiple lysine residues amenable to protection with an NPBF-group. Most notably, Lys-3 of the epitope, as its protection was found to abolish the selectivity of several FLAG-specific antibodies. The first construct that was made (Scheme **2**), contained an N-terminal sortag-motif[43] (for conjugating the tag to an anti-CD8 nanobody) followed by an NPBF-caged FLAG-tag. This molecule was next conjugated to an anti-CD8 nanobody dimer and applied to a fresh tumour sample. However, irradiation of the ROIs in the tumour at the phototoxic limit of these primary immune cells did not result in cells that could be distinguished from non-irradiated regions. A second shortcoming in this strategy was that a second fluorescent anti-CD8 antibody had to be added to identify the CD8+ T cell pool in the tumour block. This likely resulted in competition for anti-CD8 binding sites further lowering the maximal signal after deprotection.

To circumvent both of these limitations, a new strategy was devised: the photo-OR-switch (Figure **7**). Instead of irradiation leading to an off-to-on-signal, an approach was envisioned in which irradiation would remove one signal whilst simultaneously revealing the FLAG-tag. This would enable the identification of the CD8+ T cell population whilst simultaneously allowing tagging of ROIs within this population, with a single anti-CD8 nanobody dimer conjugate treatment. Furthermore, the disappearance of one signal in conjunction with the appearance of a different signal allows for a two-dimensional separation by flow cytometry.

Scheme **2** depicts the synthesis of the OR-gate probe which was conjugated to an anti-CD8 nanobody dimer. At least three N-terminal glycines were necessary in the OR-gate probe to act as a recognition motif and nucleophile in the sortase-mediated transpeptidation of the probe with a CD8 nanobody dimer. The FLAG-tag was positioned C-terminally in the peptide, of which the center Lys was designated to append the NPBF-linker onto to act as a cage against a suitable anti-FLAG antibody. An alkyne was installed as the second functionality in the NPBF-linker, which was used to click an AlexaFluor 594 group for primary detection of the CD8+ T cells. A cysteine was also included for later conjugation to a second fluorophore. This feature was, however, not exploited in the final construct.
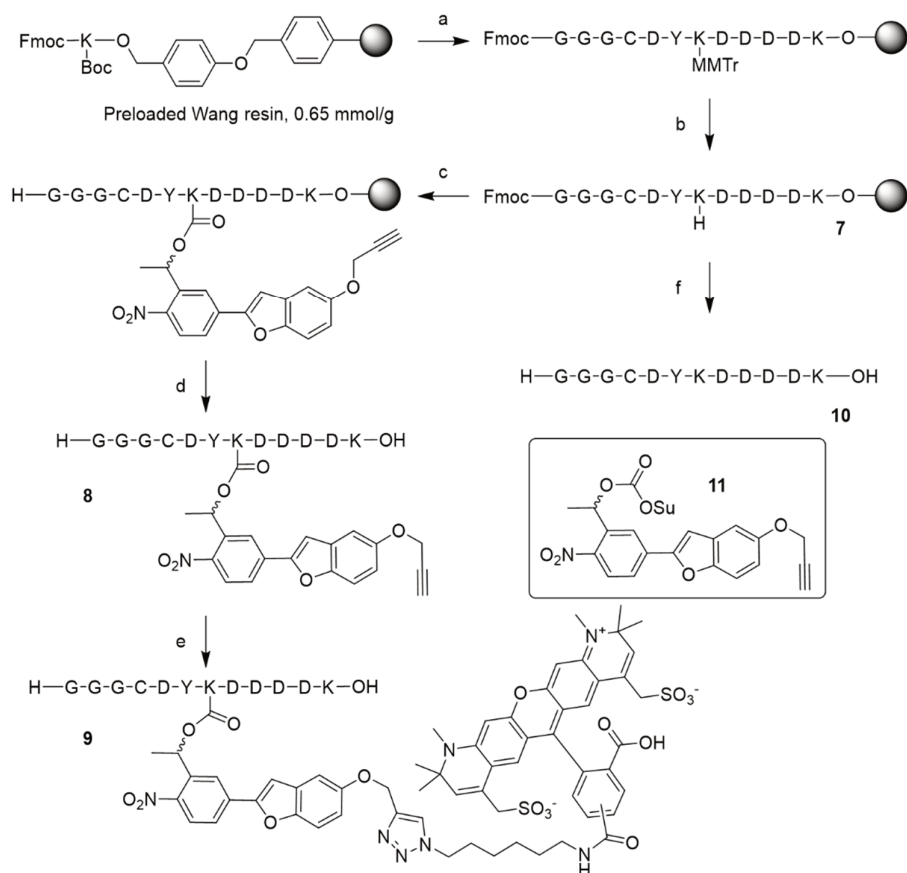
Scheme 2. **a)** HCTU-mediated Fmoc-based SPPS **b)** 1% TFA in DCM, r.t., 5 min (10 x) **c)** i) Compound **11**, DiPEA, DCM, r.t., o.n. ii) 20% Piperidine in DMF, r.t., 15 min (3 x) **d)** TFA, H$_2$O, TIS, r.t., 2 hr **e)** AF594 azide, CuI, sodium ascorbate, THPTA, DiPEA, DMSO, r.t., 4 hrs **f)** i) 20% Piperidine in DMF, r.t., 15 min (3 x) ii) TFA, H$_2$O, TIS, r.t., 2 hr.

Nonetheless, conjugate **9**, as well as free peptide **10** and photocaged-only peptide **8**, were obtained in sufficient quantities to label anti-CD8 nanobodies (αCD8^{D-1}). Using a sortase-mediated transpeptidation, αCD8^{D-1} nanobodies were conjugated with either **9** (photosensitive tag, 'PsT'), **8** or **10**. Conjugated nanobody **PsT** was then tested on an in vitro sample of CD8+ T cells (Figure **8**). In this manner the feasibility of the approach could be assessed before moving to primary tumour material.
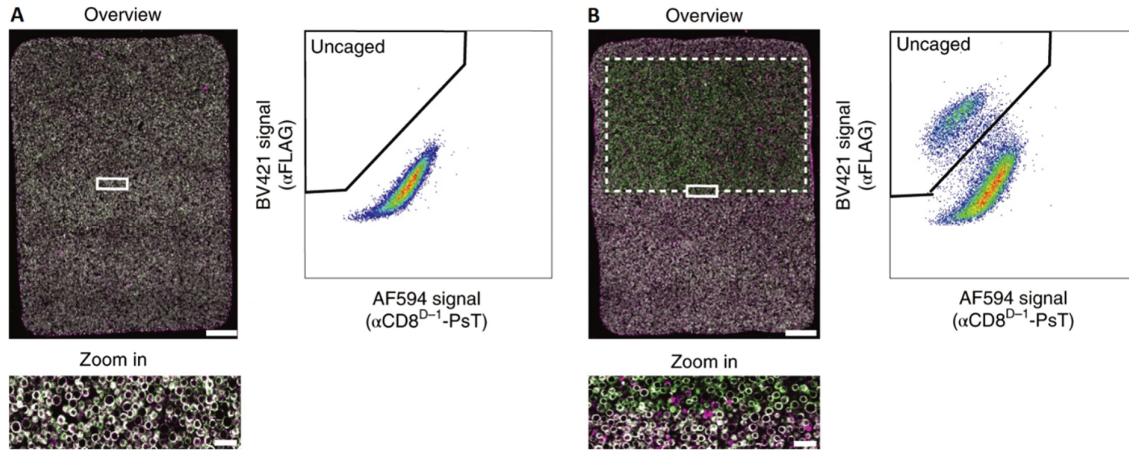
Figure 8. Uncaging of primary human CD8⁺ T cells tagged with **PsT**. A) Left: Confocal image of CD8⁺ T cells stained with **PsT** (magenta) and FITC-αCD8^D-2 (green). Overlapping signals are portrayed as white. The area within the white rectangle is shown at a higher magnification below the image. Scale bars: 100 μm (top), 10 μm (bottom). Right: flow cytometry analysis of the sample after treatment with anti-FLAG antibodies. B) Left: Confocal image of CD8⁺ T cells as in A). The area within the dashed white rectangle has been exposed to 405 nm light. The area within the solid white rectangle is shown at a higher magnification below the image. Scale bars: 100 μm (top), 10 μm (bottom). Right: flow cytometry analysis of the sample after uncaging with 405 nm light and subsequent treatment with anti-FLAG antibodies. Experiment performed by Anne van der Leun, Mirjam Hoekstra and Mireille Toebes.

The CD8⁺ T cells were treated with both **PsT** (exhibiting magenta colour) and FITC-labeled αCD8^D-2 (exhibiting green colour). Thus, in a non-irradiated sample cells are shown as white due to overlapping signals (Figure **8**A, left). Exposure to a 405 nm laser in a designated area led to the loss of the AF594 signal in the exposed area only, causing the T cells to be shown as green only (Figure **8**B, left). Flow cytometry analysis of the total sample before (Figure **8**A, right) and after (Figure **8**B, right) irradiation yields a separate population that can be gated as 'uncaged' in a quantitative manner. This probe has subsequently been used to successfully tag and isolate T-cells from ROIs in viable human melanoma and non-squamous cell lung cancer tissues, followed by the sequencing of their transcriptome.[2]

Experimental section

General methods

Commercially acquired reagents and solvents were used as received. Anhydrous solvents were prepared with activated 3 Å or 4 Å molecular sieves. All reaction progress was monitored by TLC analysis on Merck aluminum plates pre-coated with silica gel 60 and F254 fluorescent indicator; 254 nm UV light was used to check for compounds, and TLC plates were developed by charring (at approximately 150 °C) plates that were sprayed with permanganate stain (20 g/L $KMnO_4$ and 10 g/L K_2CO_3 in H_2O), unless stated otherwise. R_f values reported consider the compound being synthesized. Screening Devices silica gel (40-63 μm particle size and 60 Å pore diameter) was used during column chromatography. ^1H and ^{13}C NMR spectra were recorded on Bruker AV-400 (400 MHz) and AV-500 (500 MHz) spectrometers. Chemical shifts are reported as δ-values in ppm relative to tetramethylsilane (which was added to $CDCl_3$) or residual solvent peaks. The ^{13}C spectra are proton decoupled. LC-MS checks for all compounds were performed on a Finnigan Surveyor HPLC system with a Gemini C18 50 x 4.60 mm column, which was coupled to a Finnigan LCQ Advantage Max mass spectrometer. LC-MS samples were prepared by dissolving compounds in a tBuOH:ACN:H_2O mixture (1:1:1 by volume).
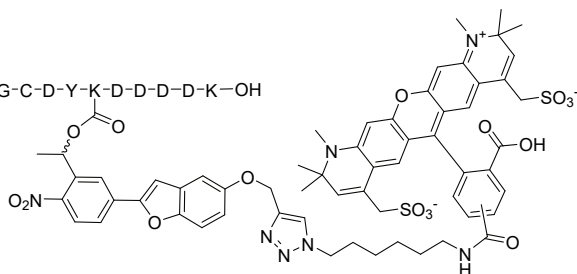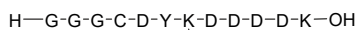
Compound 7

Fmoc—G-G-G-C-D-Y-K(H)-D-D-D-D-K—O—⬤ Preloaded Wang resin with Fmoc-Lys(Boc)-OR (0.65 mmol/g; 0.5 mmol, 0.77 g) was used as the starting material in Fmoc SPPS. Fmoc-Asp(t-Bu)-OH, Fmoc-Lys(MMTr)-OH, Fmoc-Tyr(t-Bu)-OH, Fmoc-Cys(Trt)-OH and Fmoc-Gly-OH were used as the amino acid building blocks. The following automated and repetitive sequence was used: 1) DMF wash and nitrogen purge (1x) 2) Fmoc deprotection using 20% piperidine in DMF (3x5mL) 3) DMF wash (3x) and nitrogen purge 4) Coupling of the amino acid building block (5-fold excess for amino acid, except for Fmoc-Lys(MMTr)-OH for which a 2-fold excess was used) with HCTU (5-fold excess) and DiPEA (10-fold excess) 5) DMF wash (3x) and nitrogen purge 6) Capping of unreacted amines using a mixture of Ac_2O/DiPEA/DMF (20/2/78; v/v/v) 7) DMF wash (3x). A sample (~10 mg) was taken and deprotected by agitation in a mixture of TFA/TIS/H_2O (95/2.5/2.5; v/v/v) for 3 hours. The reaction mixture was filtered and precipitated in Et_2O (-20°C). The precipitate was collected and analyzed by LC-MS (30% AcN in H_2O to 70% AcN in H_2O, C18, TFA, 13 min): R_t = 1.61 min, ESI (m/z): 1509.5 [M+H]$^+$. Monomethoxytrityl was removed by swelling the resin in DCM (1 hour), followed by treatment with 1% TFA in DCM (10x3 min.). Completion of the reaction was verified by acetylating a sample (~10 mg) using a mixture of Ac_2O/DiPEA/DMF (20/2/78; v/v/v) after which the peptide was washed with DCM (3x) and deprotected by agitation in a mixture of TFA/TIS/H_2O (95/2.5/2.5; v/v/v) for 3 hours. The reaction mixture was filtered and precipitated in Et_2O (-20°C). The precipitate was collected and analyzed by LC-MS. **LC-MS (3070, C18, H_2O/AcN + TFA, 13 min):** R_t = 2.19 min, ESI (m/z): 1552.3 [M+H]$^+$.
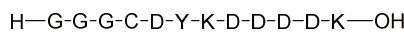
Compound 8

H—G-G-G-C-D-Y-K-D-D-D-D-K—OH
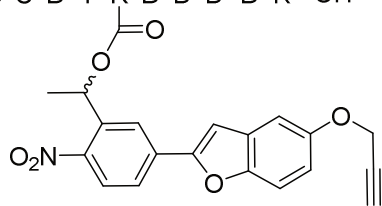
Compound **7** (25 μmol, 88 mg) was swollen in DCM (1 hour). Compound **11** (30 μmol, 16 mg) and a solution of DiPEA (100 μmol, 17 μL) in DCM (0.5 mL) was added to the resin and the reaction was shaken overnight. A sample (~5 mg) was taken and deprotected by agitation in a mixture of TFA/TIS/H$_2$O (95/2.5/2.5; v/v/v) for 3 hours. The reaction mixture was filtered and precipitated in Et$_2$O (-20°C). The precipitate was collected and analyzed by LC-MS (30% AcN in H$_2$O to 70% AcN in H$_2$O, C18, TFA, 13 min): R$_t$ = 5.78 min, ESI (m/z): 1873.5 [M+H]$^+$. After completion of the reaction was established, the resin was washed with DMF (5x). The resin was treated with a solution of 20% piperidine in DMF (3 x 10min). The resin was washed with DMF (3x) and DCM (5x). A solution of TFA/TIS/H$_2$O (95/2.5/2.5; v/v/v) was added and the mixture was shaken for 3 hours. The reaction mixture was filtered and precipitated in Et$_2$O (-20°C). The precipitate was collected and purified by RP-HPLC. **LC-MS (3070, C18, H$_2$O/AcN + TFA, 11 min):** R$_t$ = 4.23 min, ESI (m/z): 1605.5 [M+H]$^+$. **HRMS:** Calculated for C$_{70}$H$_{89}$N$_{15}$O$_{30}$S 1651.56095 [M+H]$^+$; found 1651.56094.

Compound 9

H—G-G-G-C-D-Y-K-D-D-D-D-K—OH

Compound **8** (0.5 μmol, 0.82 mg) was dissolved in DMSO (100 μL). A solution of AFDye™594 (0.5 μmol, 0.43 mg (purchased from ClickChemistryTools) in water (100 μL) was added. Solutions of CuSO$_4$ (0.1 M, 0.5 μmol, 50 μL), THPTA (0.1 M, 0.25 μmol, 2.5 μL) and ascorbic acid (1 M, 5 μmol, 5 μL) in water were purged with N$_2$ and added. The reaction was shaken under a nitrogen atmosphere for 2 hours. The reaction mixture was diluted with H$_2$O after which the precipitate was collected by centrifugation. **LC-MS (3070, C18, H$_2$O/AcN + TFA, 11 min):** R$_t$ = 2.77 min, ESI (m/z): 1249.8 [M+2H]$^{2+}$

Compound 10

H—G-G-G-C-D-Y-K-D-D-D-D-K—OH

Compound **7** was swollen in DCM (1 hour) and deprotected by agitation in a mixture of TFA/TIS/H$_2$O (95/2.5/2.5; v/v/v) for 3 hours. The reaction mixture was filtered and precipitated in Et$_2$O (-20°C). The precipitate was collected and purified by RP-HPLC. **LC-MS (3070, C18, H$_2$O/AcN + TFA, 13 min):** R$_t$ = 1.61 min, ESI (m/z): 1509.5 [M+H]$^+$.

References

(1)   Maurits, E.; van de Graaff, M. J.; Maiorana, S.; Wander, D. P. A.; Dekker, P. M.; van der Zanden, S. Y.; Florea, B. I.; Neefjes, J. J. C.; Overkleeft, H. S.; van Kasteren, S. I. Immunoproteasome Inhibitor–Doxorubicin Conjugates Target Multiple Myeloma Cells and Release Doxorubicin upon Low-Dose Photon Irradiation. *J. Am. Chem. Soc.* **2020**, *142* (16), 7250–7253.

(2)   van der Leun, A. M.; Hoekstra, M. E.; Reinalda, L.; Scheele, C. L. G. J.; Toebes, M.; van de Graaff, M. J.; Chen, L. Y. Y.; Li, H.; Bercovich, A.; Lubling, Y.; David, E.; Thommen, D. S.; Tanay, A.; van Rheenen, J.; Amit, I.; van Kasteren, S. I.; Schumacher, T. N. Single-Cell Analysis of Regions of Interest (SCARI) Using a Photosensitive Tag. *Nat. Chem. Biol.* **2021**, *17* (11), 1139–1147.

(3)   Savva, A.; Roger, T. Targeting Toll-Like Receptors: Promising Therapeutic Strategies for the Management of Sepsis-Associated Pathology and Infectious Diseases. *Front. Immunol.* **2013**, *4*.

(4)   Hennessy, E. J.; Parker, A. E.; O'Neill, L. A. J. Targeting Toll-like Receptors: Emerging Therapeutics? *Nat. Rev. Drug Discov.* **2010**, *9* (4), 293–307.

(5)   Braunstein, M. J.; Kucharczyk, J.; Adams, S. Targeting Toll-Like Receptors for Cancer Therapy. *Target. Oncol.* **2018**, *13* (5), 583–598.

(6)   Tsujimoto, H.; Ono, S.; Efron, P. A.; Scumpia, P. O.; Moldawer, L. L.; Mochizuki, H. ROLE OF TOLL-LIKE RECEPTORS IN THE DEVELOPMENT OF SEPSIS: *Shock* **2007**, 1.

(7)   Zuo, L.; Lucas, K.; Fortuna, C. A.; Chuang, C.-C.; Best, T. M. Molecular Regulation of Toll-like Receptors in Asthma and COPD. *Front. Physiol.* **2015**, *6*.

(8)   Lafyatis, R.; Marshak-Rothstein, A. Toll-like Receptors and Innate Immune Responses in Systemic Lupus Erythematosus. *Arthritis Res. Ther.* **2007**, *9* (6), 222.

(9)   Park, B.; Brinkmann, M. M.; Spooner, E.; Lee, C. C.; Kim, Y.-M.; Ploegh, H. L. Proteolytic Cleavage in an Endolysosomal Compartment Is Required for Activation of Toll-like Receptor 9. *Nat. Immunol.* **2008**, *9* (12), 1407–1414.

(10)   Maschalidi, S.; Hässler, S.; Blanc, F.; Sepulveda, F. E.; Tohme, M.; Chignard, M.; van Endert, P.; Si-Tahar, M.; Descamps, D.; Manoury, B. Asparagine Endopeptidase Controls Anti-Influenza Virus Immune Responses through TLR7 Activation. *PLoS Pathog.* **2012**, *8* (8), e1002841.

(11)   Ewald, S. E.; Engel, A.; Lee, J.; Wang, M.; Bogyo, M.; Barton, G. M. Nucleic Acid Recognition by Toll-like Receptors Is Coupled to Stepwise Processing by Cathepsins and Asparagine Endopeptidase. *J. Exp. Med.* **2011**, *208* (4), 643–651.

(12)   Garcia-Cattaneo, A.; Gobert, F.-X.; Muller, M.; Toscano, F.; Flores, M.; Lescure, A.; Del Nery, E.; Benaroch, P. Cleavage of Toll-like Receptor 3 by Cathepsins B and H Is Essential for Signaling. *Proc. Natl. Acad. Sci.* **2012**, *109* (23), 9053–9058.

(13)   Marre, M. L.; Petnicki-Ocwieja, T.; DeFrancesco, A. S.; Darcy, C. T.; Hu, L. T. Human Integrin A3β1 Regulates TLR2 Recognition of Lipopeptides from Endosomal Compartments. *PLoS ONE* **2010**, *5* (9), e12871.

(14)   Mancini, R. J.; Stutts, L.; Moore, T.; Esser-Kahn, A. P. Controlling the Origins of Inflammation with a Photoactive Lipopeptide Immunopotentiator. *Angew. Chem. Int. Ed.* **2015**, *54* (20), 5962–5965.

(15) Ryu, K. A.; Stutts, L.; Tom, J. K.; Mancini, R. J.; Esser-Kahn, A. P. Stimulation of Innate Immune Cells by Light-Activated TLR7/8 Agonists. *J. Am. Chem. Soc.* **2014**, *136* (31), 10823–10825.

(16) Stutts, L.; Esser-Kahn, A. P. A Light-Controlled TLR4 Agonist and Selectable Activation of Cell Subpopulations. *ChemBioChem* **2015**, *16* (12), 1744–1748.

(17) Govan, J. M.; Young, D. D.; Lively, M. O.; Deiters, A. Optically Triggered Immune Response through Photocaged Oligonucleotides. *Tetrahedron Lett.* **2015**, *56* (23), 3639–3642.

(18) Jemas, A.; Xie, Y.; Pigga, J. E.; Caplan, J. L.; am Ende, C. W.; Fox, J. M. Catalytic Activation of Bioorthogonal Chemistry with Light (CABL) Enables Rapid, Spatiotemporally Controlled Labeling and No-Wash, Subcellular 3D-Patterning in Live Cells Using Long Wavelength Light. *J. Am. Chem. Soc.* **2022**, *144* (4), 1647–1662.

(19) Yu, D.; Kandimalla, E. R.; Bhagat, L.; Tang, J.-Y.; Cong, Y.; Tang, J.; Agrawal, S. `Immunomers' novel 3'- 3' Linked CpG Oligodeoxyribonucleotides as Potent Immunomodulatory Agents. *Nucleic Acid Res. 30* (20), 4460–4469.

(20) Komori, N.; Jakkampudi, S.; Motoishi, R.; Abe, M.; Kamada, K.; Furukawa, K.; Katan, C.; Sawada, W.; Takahashi, N.; Kasai, H.; Xue, B.; Kobayashi, T. Design and Synthesis of a New Chromophore, 2-(4-Nitrophenyl)Benzofuran, for Two-Photon Uncaging Using near-IR Light. *Chem. Commun.* **2016**, *52* (2), 331–334.

(21) Lu, J.; Jiang, F.; Lu, A.; Zhang, G. Linkers Having a Crucial Role in Antibody–Drug Conjugates. *Int. J. Mol. Sci.* **2016**, *17* (4), 561.

(22) Trail, P.; Willner, D.; Lasch, S.; Henderson, A.; Hofstead, S.; Casazza, A.; Firestone, R.; Hellstrom, I.; Hellstrom, K. Cure of Xenografted Human Carcinomas by BR96-Doxorubicin Immunoconjugates. *Science* **1993**, *261* (5118), 212–215.

(23) Kellogg, B. A.; Garrett, L.; Kovtun, Y.; Lai, K. C.; Leece, B.; Miller, M.; Payne, G.; Steeves, R.; Whiteman, K. R.; Widdison, W.; Xie, H.; Singh, R.; Chari, R. V. J.; Lambert, J. M.; Lutz, R. J. Disulfide-Linked Antibody–Maytansinoid Conjugates: Optimization of In Vivo Activity by Varying the Steric Hindrance at Carbon Atoms Adjacent to the Disulfide Linkage. *Bioconjug. Chem.* **2011**, *22* (4), 717–727.

(24) Spangler, B.; Kline, T.; Hanson, J.; Li, X.; Zhou, S.; Wells, J. A.; Sato, A. K.; Renslo, A. R. Toward a Ferrous Iron-Cleavable Linker for Antibody–Drug Conjugates. *Mol. Pharm.* **2018**, *15* (5), 2054–2059.

(25) Rossin, R.; van Duijnhoven, S. M. J.; ten Hoeve, W.; Janssen, H. M.; Kleijn, L. H. J.; Hoeben, F. J. M.; Versteegen, R. M.; Robillard, M. S. Triggered Drug Release from an Antibody–Drug Conjugate Using Fast "Click-to-Release" Chemistry in Mice. *Bioconjug. Chem.* **2016**, *27* (7), 1697–1706.

(26) Versteegen, R. M.; Rossin, R.; ten Hoeve, W.; Janssen, H. M.; Robillard, M. S. Click to Release: Instantaneous Doxorubicin Elimination upon Tetrazine Ligation. *Angew. Chem. Int. Ed.* **2013**, *52* (52), 14112–14116.

(27) Rossin, R.; Versteegen, R. M.; Wu, J.; Khasanov, A.; Wessels, H. J.; Steenbergen, E. J.; ten Hoeve, W.; Janssen, H. M.; van Onzen, A. H. A. M.; Hudson, P. J.; Robillard, M. S. Chemically Triggered Drug Release from an Antibody-Drug Conjugate Leads to Potent Antitumour Activity in Mice. *Nat. Commun.* **2018**, *9* (1), 1484.

(28) Wang, Y.; Cheetham, A. G.; Angacian, G.; Su, H.; Xie, L.; Cui, H. Peptide–Drug Conjugates as Effective Prodrug Strategies for Targeted Delivery. *Adv. Drug Deliv. Rev.* **2017**, *110–111*, 112–126.

(29) de Bruin, G.; Huber, E. M.; Xin, B.-T.; van Rooden, E. J.; Al-Ayed, K.; Kim, K.-B.; Kisselev, A. F.; Driessen, C.; van der Stelt, M.; van der Marel, G. A.; Groll, M.; Overkleeft, H. S. Structure-Based Design of B1i or B5i Specific Inhibitors of Human Immunoproteasomes. *J. Med. Chem.* **2014**, *57* (14), 6197–6209.

(30) Chen, M.; Pennathur, A.; Luketich, J. D. Role of Photodynamic Therapy in Unresectable Esophageal and Lung Cancer. *Lasers Surg. Med.* **2006**, *38* (5), 396–402.

(31) Thommen, D. S.; Schumacher, T. N. T Cell Dysfunction in Cancer. *Cancer Cell* **2018**, *33* (4), 547–562.

(32) Keren, L.; Bosse, M.; Thompson, S.; Risom, T.; Vijayaragavan, K.; McCaffrey, E.; Marquez, D.; Angoshtari, R.; Greenwald, N. F.; Fienberg, H.; Wang, J.; Kambham, N.; Kirkwood, D.; Nolan, G.; Montine, T. J.; Galli, S. J.; West, R.; Bendall, S. C.; Angelo, M. MIBI-TOF: A Multiplexed Imaging Platform Relates Cellular Phenotypes and Tissue Structure. *Sci. Adv.* **2019**, *5* (10), eaax5851.

(33) Goltsev, Y.; Samusik, N.; Kennedy-Darling, J.; Bhate, S.; Hale, M.; Vazquez, G.; Black, S.; Nolan, G. P. Deep Profiling of Mouse Splenic Architecture with CODEX Multiplexed Imaging. *Cell* **2018**, *174* (4), 968-981.e15.

(34) Medaglia, C.; Giladi, A.; Stoler-Barak, L.; De Giovanni, M.; Salame, T. M.; Biram, A.; David, E.; Li, H.; Iannacone, M.; Shulman, Z.; Amit, I. Spatial Reconstruction of Immune Niches by Combining Photoactivatable Reporters and ScRNA-Seq. *Science* **2017**, *358* (6370), 1622–1626.

(35) Moncada, R.; Barkley, D.; Wagner, F.; Chiodin, M.; Devlin, J. C.; Baron, M.; Hajdu, C. H.; Simeone, D. M.; Yanai, I. Integrating Microarray-Based Spatial Transcriptomics and Single-Cell RNA-Seq Reveals Tissue Architecture in Pancreatic Ductal Adenocarcinomas. *Nat. Biotechnol.* **2020**, *38* (3), 333–342.

(36) Vickovic, S.; Eraslan, G.; Salmén, F.; Klughammer, J.; Stenbeck, L.; Schapiro, D.; Äijö, T.; Bonneau, R.; Bergenstråhle, L.; Navarro, J. F.; Gould, J.; Griffin, G. K.; Borg, Å.; Ronaghi, M.; Frisén, J.; Lundeberg, J.; Regev, A.; Ståhl, P. L. High-Definition Spatial Transcriptomics for in Situ Tissue Profiling. *Nat. Methods* **2019**, *16* (10), 987–990.

(37) Thrane, K.; Eriksson, H.; Maaskola, J.; Hansson, J.; Lundeberg, J. Spatially Resolved Transcriptomics Enables Dissection of Genetic Heterogeneity in Stage III Cutaneous Malignant Melanoma. *Cancer Res.* **2018**, canres.0747.2018.

(38) Maniatis, S.; Äijö, T.; Vickovic, S.; Braine, C.; Kang, K.; Mollbrink, A.; Fagegaltier, D.; Andrusivová, Ž.; Saarenpää, S.; Saiz-Castro, G.; Cuevas, M.; Watters, A.; Lundeberg, J.; Bonneau, R.; Phatnani, H. Spatiotemporal Dynamics of Molecular Pathology in Amyotrophic Lateral Sclerosis. *Science* **2019**, *364* (6435), 89–93.

(39) Berglund, E.; Maaskola, J.; Schultz, N.; Friedrich, S.; Marklund, M.; Bergenstråhle, J.; Tarish, F.; Tanoglidi, A.; Vickovic, S.; Larsson, L.; Salmén, F.; Ogris, C.; Wallenborg, K.; Lagergren, J.; Ståhl, P.; Sonnhammer, E.; Helleday, T.; Lundeberg, J. Spatial Maps of Prostate Cancer Transcriptomes Reveal an Unexplored Landscape of Heterogeneity. *Nat. Commun.* **2018**, *9* (1), 2419.

(40) Ståhl, P. L.; Salmén, F.; Vickovic, S.; Lundmark, A.; Navarro, J. F.; Magnusson, J.; Giacomello, S.; Asp, M.; Westholm, J. O.; Huss, M.; Mollbrink, A.; Linnarsson, S.;

Codeluppi, S.; Borg, Å.; Pontén, F.; Costea, P. I.; Sahlén, P.; Mulder, J.; Bergmann, O.; Lundeberg, J.; Frisén, J. Visualization and Analysis of Gene Expression in Tissue Sections by Spatial Transcriptomics. *Science* **2016**, *353* (6294), 78–82.

(41) Rodriques, S. G.; Stickels, R. R.; Goeva, A.; Martin, C. A.; Murray, E.; Vanderburg, C. R.; Welch, J.; Chen, L. M.; Chen, F.; Macosko, E. Z. Slide-Seq: A Scalable Technology for Measuring Genome-Wide Expression at High Spatial Resolution. **2019**, 6.

(42) Hu, K. H.; Eichorst, J. P.; McGinnis, C. S.; Patterson, D. M.; Chow, E. D.; Kersten, K.; Jameson, S. C.; Gartner, Z. J.; Rao, A. A.; Krummel, M. F. ZipSeq: Barcoding for Real-Time Mapping of Single Cell Transcriptomes. *Nat. Methods* **2020**, *17* (8), 833–843.

(43) Popp, M. W.; Antos, J. M.; Grotenbreg, G. M.; Spooner, E.; Ploegh, H. L. Sortagging: A Versatile Method for Protein Labeling. *Nat. Chem. Biol.* **2007**, *3* (11), 707–708.